Frequency-Tuned Approaches to Wall Transpiration Control

Anushka Subedi* and Yulia Peet†
School for Engineering of Matter, Transport and Energy, Arizona State University, Tempe, AZ, 85281

Improving turbulent flow control is crucial for various applications like reducing drag, enhancing mixing, and managing heat transfer. Feedback control approaches, which sense the turbulent signal in the flow and modify the actuation depending on the value of the signal, such as opposition control or a wall-sensing control, have proven to be effective. However, these approaches use the full, unfiltered signal, which naturally contains multiple frequencies. In conjunction with a recent interest in passive frequency-tuned surfaces that selectively respond to a single frequency or a band of frequencies, this paper explores a feedback-control approach that focuses on specific frequencies. We compare the frequency-tuned approach with the classical opposition control (that senses flow velocity in some off-wall location) and with our previously-developed wall-sensing control (that acts upon a wall shear stress), both using unfiltered temporal signals (across all frequencies). Initial findings show a drag reduction of 21.11% at $Re_\tau \approx 180$ and 18% at $Re_\tau \approx 390$ using classical opposition control, and 10.64% at $Re_\tau \approx 180$ and 7.12% at $Re_\tau \approx 390$ using wall-sensing control, demonstrating some reduction in effectiveness for wall-sensing strategy. The frequency-tuned method developed in this study achieved only modest drag reductions, ranging between 1% and 2% for $Re_\tau \approx 180$, and even showed a slight drag increase of 1% to 2% with higher Reynolds numbers ($Re_\tau \approx 390$). This outcome highlights the limitations of relying on a single-frequency control strategy, which proves inadequate for managing complex turbulence dynamics that has a broadband spectrum, especially at higher Reynolds numbers.

I. Nomenclature

Re_τ	=	viscous Reynold's number
DNS	=	Direct Numerical Simulation
CFL	=	Courant–Friedrichs–Lewy
u_y	=	vertical velocity
u_x	=	streamline velocity
$\tau = \nu \frac{\partial u_x}{\partial y}$	=	instantaneous shear stress
$u'_y u'_y$	=	Reynold's velocity stress term in y-direction
$\nu^2 \frac{\partial u'_x}{\partial y} \frac{\partial u'_x}{\partial y}$	=	averaged wall shear stress fluctuation
ω_c	=	control frequency
DR	=	drag reduction
K	=	control gain
A	=	amplitude referred in wall-sensing control
T^+	=	time in wall units

II. Introduction

In various engineering domains, such as aerospace, automotive, and marine systems, mitigating skin friction drag is a critical challenge due to its significant impact on energy consumption and operational efficiency. High drag levels not only increase fuel usage but also limit the performance capabilities of systems, from aircraft to underwater vessels. For instance, even small improvements in drag reduction for commercial aircraft can lead to significant fuel savings, lower

*Ph.D. Student, AIAA member, email: asubedi5@asu.edu
†Associate Professor, AIAA member, email: ypeet@asu.edu

greenhouse gas emissions, and reduced operational costs. Addressing this issue has motivated researchers to explore various drag reduction strategies, which broadly fall into two categories: active and passive control techniques.

Active control strategies involve directly manipulating the flow dynamics using energy-intensive mechanisms. These methods include blowing and suction [1–4], synthetic jets [5, 6], and fluidic oscillators [7]. Such approaches enable precise control over turbulent structures, thereby reducing skin friction drag effectively. For example, synthetic jets introduce oscillatory flows that disrupt turbulence near walls, reducing energy losses. However, the reliance of these strategies on external energy input and the complexity of their control systems often limit their large-scale practical applications, especially in energy-conscious industries.

Conversely, passive control strategies aim to achieve drag reduction without requiring continuous energy input, offering a more sustainable alternative. Traditional passive methods, such as compliant surfaces and retrofitting [8], modify flow boundary conditions to influence turbulence behavior. Recent advancements in material science have introduced the concept of metamaterials, which are architectured surfaces designed to manipulate mechanical wave behavior, such as inhibiting or amplifying specific frequency components of wall shear stress [9, 10]. Metamaterials can provide a unique advantage by tailoring surface properties to interact with flow dynamics passively, opening pathways for innovative, energy-efficient drag reduction techniques.

In our previous study, we compared the effectiveness of two active feedback control strategies: a well-established opposition control methodology and a wall-sensing approach [11]. Opposition control employs vertical velocity measurements taken at an off-wall location to generate a control input that counteracts near-wall turbulence. This method demonstrated substantial drag reductions, achieving 21.11% at $Re_\tau \approx 180$ and 18% at $Re_\tau \approx 390$. In contrast, the wall-sensing approach, which relies on wall shear stress measurements to generate control inputs, achieved more modest reductions of 10.64% and 7.12% at the same Reynolds numbers. A critical limitation of the wall-sensing method was its susceptibility to instabilities, likely caused by high-frequency components in the fluctuating shear stress signal.

While opposition and wall-sensing control approaches, previously explored via numerical simulations [1, 11], use the full, unfiltered, instantaneous signal that naturally contains multiple frequencies, in practical applications it may be difficult to sense or actuate at a large range of frequencies, and a single frequency or a band of frequencies may often need to be targeted. Examples include a recently proposed concept of metamaterials for flow control, which have certain frequency bandgaps that define their response characteristics [9, 10]. In view of these practical applications, the current study implements a frequency-tuned control approach within both opposition-control and wall-sensing control frameworks. To define a frequency-tuned control signal, we introduce a filtering approach to an instantaneous signal which extracts a specific frequency content that is used to define the wall actuation velocity.

The methodology is evaluated using Direct Numerical Simulations (DNS) conducted with the high-order Spectral Element code Nek5000 [12, 13]. The results compare the performance of frequency-tuned and untuned control strategies, highlighting their relative efficacy. The frequency-tuned method we developed yielded only modest drag reductions, limited to a range of 1% to 2% across all cases. This result highlights the inherent limitations of employing a single-frequency control approach. To overcome these limitations, future efforts will target multiple frequencies or a band of frequencies, aiming to capture a broader range of turbulence dynamics and improve the overall effectiveness of the control strategy.

III. Methods

The Direct Numerical Simulations of the frequency-tuned and untuned flow control methodologies are conducted utilizing the Spectral Element code, Nek5000 [14], in its incompressible formulation. Nek5000 is distinguished as a high-order code employing Lagrange interpolating polynomial basis functions defined on the Gauss-Lobatto points. This configuration guarantees efficient tensor-product utilization and rapid convergence.

A turbulent channel flow is utilized as a model geometry in this work. The size of the domain is set to $2\pi h \times 2h \times \pi h$, where h is the channel half-width. Boundary conditions for the channel flow DNS are set as periodic in streamwise and spanwise directions. The bulk mean velocity, U_{bulk}, is kept constant throughout the simulations. The top and bottom walls are set as no-slip in the uncontrolled case, while the vertical wall transpiration velocity is applied to the bottom wall in the controlled case. Reynolds numbers of $Re_\tau \approx 180$ and $Re_\tau \approx 390$ are investigated. Re_τ is defined based on the uncontrolled case with the same bulk mean velocity as the controlled case, meaning that the actual Re_τ in the controlled case will vary based on the drag reduction values. The computational grid for both Reynolds numbers uses $16 \times 12 \times 8$ number of elements, each containing 8^3 Gauss-Lobatto collocation points, yielding a polynomial order of approximately $N = 7$ in the simulations. The time-step size is set to $\Delta t = 10^{-4}$, while the actual time step may slightly vary around this number to keep the CFL number constant at CFL = 0.5. To authenticate the uncontrolled base case, we

draw comparisons with the DNS data from [15] in [11]. This comparison confirmed the adequacy of the grid resolution for both Reynolds numbers. Further grid refinement studies will be documented in the final paper.

The current study considers two flow control strategies: opposition control [1] and wall-sensing control [11]. The two methodologies are first presented in their baseline, and then the frequency-tuned formulation for both the opposition control and the wall-sensing control methods are presented.

A. Opposition control

In the opposition control [1], instantaneous vertical velocity signal is sampled at a designated horizontal plane located at the distance d from the wall, $u_y(x, y = d, z, t)$, and resupplied, with the opposite sign, as a wall transpiration velocity directly underneath the sample point:

$$u_y|_{wall}(x, z, t) = u_y(x, y = 0, z, t) = -u_y(x, y = d, z, t). \tag{1}$$

B. Wall-sensing control

For the wall-sensing control method developed in our previous work [11], the following control relation is implemented:

$$u_y|_{wall}(x, z, t) = K \times \left[\left(\nu \frac{\partial u_x}{\partial y} \right)_{wall} (x, z, t) - \overline{\left(\nu \frac{\partial u_x}{\partial y} \right)_{wall}} (t) \right] \times \frac{\sqrt{\left\langle u'_y u'_y \right\rangle}^{no-control}_{y=d}}{\sqrt{\nu^2 \left\langle \frac{\partial u'_x}{\partial y} \frac{\partial u'_x}{\partial y} \right\rangle}^{no-control}_{wall}} \tag{2}$$

Here, $u_y|_{wall}(x, z, t)$ is the instantaneous vertical velocity at the wall, $\left(\nu \frac{\partial u_x}{\partial y} \right)_{wall} (x, z, t)$ is the instantaneous shear stress at the wall, $\overline{\left(\nu \frac{\partial u_x}{\partial y} \right)_{wall}} (t)$ is the plane-averaged instantaneous shear stress at the wall, $\sqrt{\left\langle u'_y u'_y \right\rangle}^{no-control}_{y=d}$ is the square root of the Reynolds stress term in the y-direction at a specified wall-normal location $y = d$ taken from the uncontrolled case with the same Reynolds number, $\sqrt{\nu^2 \left\langle \frac{\partial u'_x}{\partial y} \frac{\partial u'_x}{\partial y} \right\rangle}^{no-control}_{wall}$ is the averaged wall shear stress fluctuation taken from the uncontrolled case (angular brackets denote time and horizontal averaging), and K is the control gain. The last term in Eq. (2) is introduced to scale the control input for the transpiration velocity in accordance with the opposition control law. Even with this scaling, the control gain still needs to be adjusted as will be discussed later.

C. Frequency-Tuned Opposition Control

To develop the frequency-tuned control approach, we start with the opposition control method. The idea is to decompose the temporally varying velocity signal $v_{xdz}(t) = u_y(x, y = d, z, t)$ into its corresponding frequency components using a Fourier transform. The Fourier transform of the signal is defined as:

$$\widehat{V}_{xdz}(\omega) = \mathcal{F}\{v_{xdz}\}(\omega) = \frac{1}{2\pi} \int_{-\infty}^{\infty} v_{xdz}(t) e^{-i\omega t} \, dt, \tag{3}$$

where ω is the angular frequency. A specific control frequency $\omega = \omega_c$ is selected, and the component of the original signal corresponding to this frequency is extracted as:

$$v^{\omega_c}_{xdz}(t) = \mathcal{F}^{-1}\{\widehat{V}_{xdz}(\omega)\delta(\omega - \omega_c)\}(t) = \widehat{V}_{xdz}(\omega_c) e^{i\omega_c t}. \tag{4}$$

The frequency-adjusted wall velocity for opposition control is then defined as

$$u_y|_{\text{wall}}(x, z, t) = -K \cdot \left(v^{\omega_c}_{xdz}(t) + v^{-\omega_c}_{xdz}(t) + v^{0}_{xdz}(t) \right), \tag{5}$$

where K is the amplitude gain. In Eq. (5), we sum the signals with positive and negative frequencies, $\pm\omega_c$, to ensure the real value of the reconstructed signal, and add a mean component (corresponding to the frequency of zero). This is done in order to ensure that the signal is centered around a correct nominal value.

D. Frequency-Tuned Wall-Sensing Control

In the frequency-tuned wall-sensing control, the wall shear stress signal is filtered similarly. The frequency-filtered wall shear stress is defined as:

$$\left(\nu\frac{\partial u_x}{\partial y}\right)^{\omega_c}_{\text{wall}}(x,z,t) = \mathcal{F}^{-1}\left\{\mathcal{F}\left\{\left(\nu\frac{\partial u_x}{\partial y}\right)_{\text{wall}}\right\}(\omega_c)\right\} = \widehat{\left(\nu\frac{\partial u_x}{\partial y}\right)}_{\text{wall}} e^{i\omega_c t}. \tag{6}$$

As with the frequency-tuned opposition control, we sum the extracted signals at $\omega = \omega_c$, $\omega = -\omega_c$ and $\omega = 0$, to obtain the filtered signal as:

$$\left(\nu\frac{\partial u_x}{\partial y}\right)^{\text{filt}}_{\text{wall}}(x,z,t) = \left(\nu\frac{\partial u_x}{\partial y}\right)^{\omega_c}_{\text{wall}}(x,z,t) + \left(\nu\frac{\partial u_x}{\partial y}\right)^{-\omega_c}_{\text{wall}}(x,z,t) + \left(\nu\frac{\partial u_x}{\partial y}\right)^{0}_{\text{wall}}(x,z,t) \tag{7}$$

This frequency-filtered signal is then used in the control law as:

$$u_y|_{\text{wall}}(x,z,t) = K\cdot\left[\left(\nu\frac{\partial u_x}{\partial y}\right)^{\text{filt}}_{\text{wall}}(x,z,t) - \overline{\left(\nu\frac{\partial u_x}{\partial y}\right)}^{\text{filt}}_{\text{wall}}(t)\right]\cdot\frac{\sqrt{\langle u_y' u_y'\rangle^{\text{no-control}}_{y=d}}}{\sqrt{\nu^2\langle(\frac{\partial u_x'}{\partial y})^2\rangle^{\text{no-control}}_{\text{wall}}}}, \tag{8}$$

where $\overline{\left(\nu\frac{\partial u_x}{\partial y}\right)}^{\text{filt}}_{\text{wall}}(t)$ is the plane-averaged filtered wall shear stress, and K is the control gain.

IV. Results

A. Opposition control

The results from the opposition control, showing the evolution of drag over time at the bottom wall for $Re_\tau \approx 180$ and $Re_\tau \approx 390$, are presented in Figure (1) and Figure (2), respectively. Drag is defined here as the plane-averaged value of wall shear stress,

$$\tau_w(t) = \overline{\left(\nu\frac{\partial u_x}{\partial y}\right)}_{wall}(t) \tag{9}$$

Drag reduction is defined as

$$DR = \frac{\int_{T_1}^{T_2}\left(\tau_w^{nc}(t) - \tau_w^{c}\right)dt}{\int_{T_1}^{T_2}\tau_w^{nc}(t)dt}\cdot 100\%, \tag{10}$$

where, τ_w^{nc} corresponds to the uncontrolled case, τ_w^c to the controlled case, and $T_1 = 50$, $T_2 = 400$, normalized with h/U_{bulk}, are the start and the end of the period for collecting statistics. The maximum drag reduction achieved is 21.11% for $Re_\tau \approx 180$ with the velocity sensed at y+ value of 15 across all frequency bands. The drag reduction for y+ values of 20 is 17.94%, for y+=10 it is 16.35%, and for y+=5 it is 7.56%, showing that y+=15 gives an optimum value of drag reduction, consistent with the previous literature [16–18].

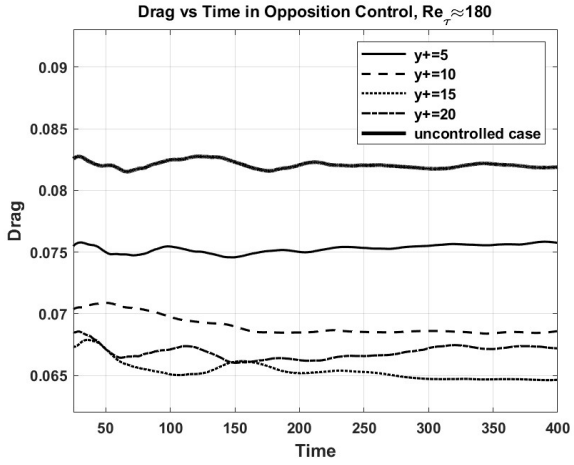

Fig. 1 Temporal evolution of drag, $\mathrm{Re}_\tau \approx 180$

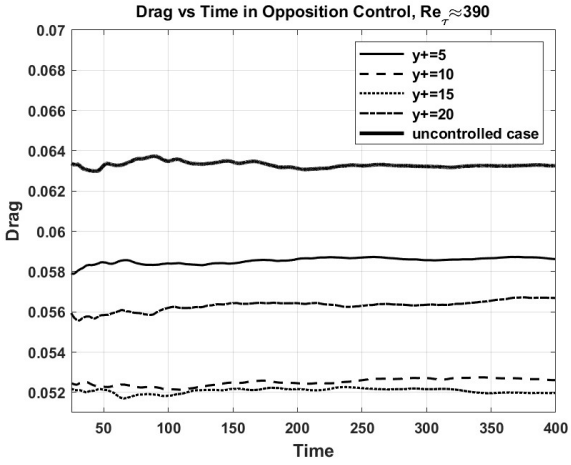

Fig. 2 Temporal evolution of drag, $\mathrm{Re}_\tau \approx 390$

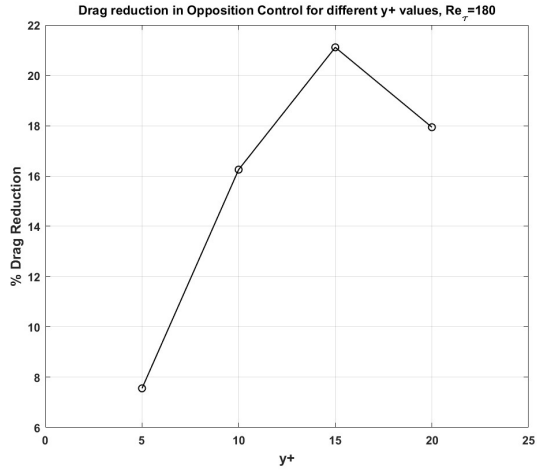

Fig. 3 Drag reduction vs y+ values for $\mathrm{Re}_\tau \approx 180$

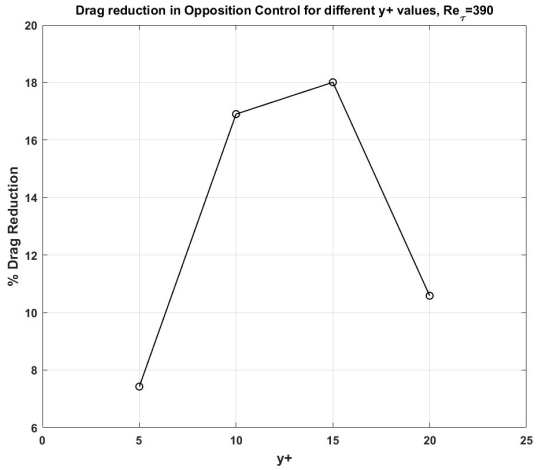

Fig. 4 Drag reduction vs y+ values for $\mathrm{Re}_\tau \approx 390$

Similarly, the maximum drag reduction achieved is 18% for $Re_\tau \approx 390$, with the velocity sensed at y+ value of 15 across all frequency bands. The drag reduction for y+ values of 10 is 16.90%, for y+=20, it is 10.58%, and for y+=5, it is 7.42%. As with $Re_\tau \approx 180$, y+=15 corresponds to the optimum wall-sensing location in our simulations. The % DR with respective sensed y+ location for $Re_\tau \approx 180$ and $Re_\tau \approx 390$ are shown in Figure (3) and Figure (4) respectively.

B. Wall-sensing control

The results from the wall-sensing flow control, showing the evolution of drag over time for $Re_\tau \approx 180$ and $Re_\tau \approx 390$, are shown in Figure (5) and Figure (6), respectively. Since the wall shear-stress signal is significantly more oscillatory than the vertical velocity signal in the opposition control, the control gain K in the wall-sensing control needs to be adjusted as $K = \alpha \cdot A$, where $\alpha = 10^{-3}$ for stability, and $A \sim O(1)$ is referred to as the amplitude. With the amplitude $A = 1$, we achieve a low drag reduction value of only 2.93% at $Re_\tau \approx 180$ and 1.12% at $Re_\tau \approx 390$. Increasing the amplitude results in higher drag reduction values, e.g., 5.38% with $A = 4$ at $Re_\tau \approx 180$ and 3.48% at $Re_\tau \approx 390$. Unfortunately, increasing the gain further resulted in an unstable control. To remedy the situation, a "freeze" strategy was implemented, where the control input was hold fixed for every 3 time steps and varied again at the end of the 3$^{\text{rd}}$ time step, and so on. With this strategy, we were able to increase the amplitude to $A = 65$ and achieve the drag reduction of 10.64% for $Re_\tau \approx 180$ and 7.12% for $Re_\tau \approx 390$. We also remark that negative gains (as expected) resulted in drag increase in wall-sensing approaches.

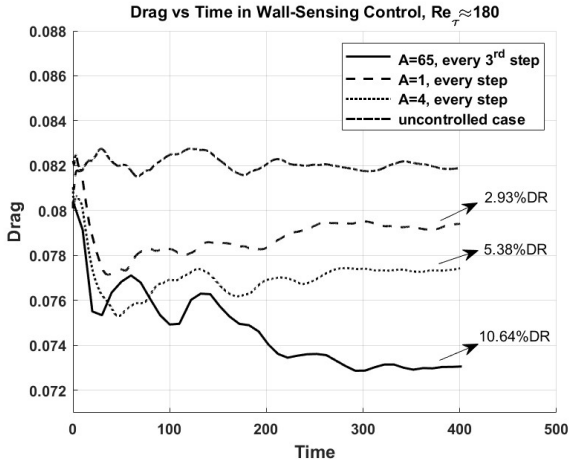

Fig. 5 Temporal evolution of drag, $\mathrm{Re}_\tau \approx 180$

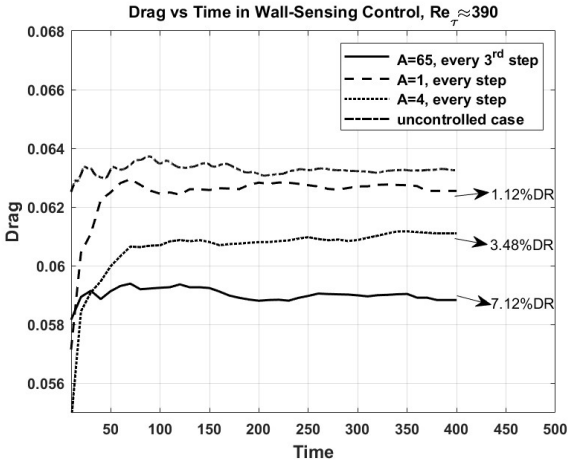

Fig. 6 Temporal evolution of drag, $\mathrm{Re}_\tau \approx 390$

The evolution of drag over time for the best identified cases from both control strategies (opposition and wall-sensing), compared to the uncontrolled base case for $Re_\tau \approx 180$ and $Re_\tau \approx 390$, is shown in Figure (7) and Figure (8), respectively. For $Re_\tau \approx 180$, there is a maximum drag reduction of 21.11% using opposition control and 10.64% using wall-sensing control. Similarly, for $Re_\tau \approx 390$, there is a maximum drag reduction of 18% using opposition control and 7.12% using the wall-sensing control.

A lower effectiveness of the wall-sensing control as opposed to the opposition control was attributed to high-frequency oscillations in the wall shear-stress signal necessitating using lower gains and thus limiting the achievable drag reduction values with this approach, see Ref. [11].

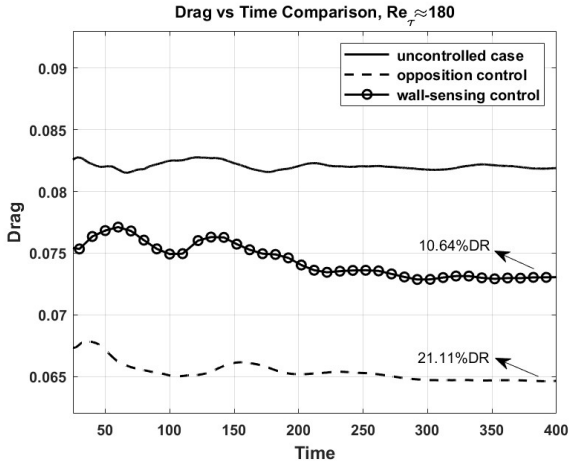

Fig. 7 $\mathrm{Re}_\tau \approx 180$

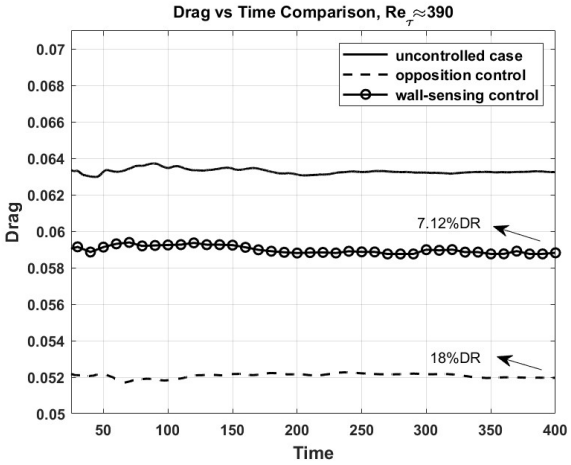

Fig. 8 $\mathrm{Re}_\tau \approx 390$

Fig. 7 and 8: Comparison between uncontrolled case, and best performing opposition control and wall-sensing control methods

C. Frequency-tuned opposition control

The results from the frequency-tuned opposition control, showing the evolution of drag over time for $Re_\tau \approx 180$ and $Re_\tau \approx 390$ are shown in Figures (9) and (10). The amplitude gain of K=300 was used for the frequency-tuned wall-sensing control. We examine six different filtering frequencies defined as:

$$\omega_c^+ = 2\pi/T^+, \tag{11}$$

where T^+ is the period of the signal in wall units. The signal periods that were investigated are categorized into three groups: short ($T^+ = 0.2$ and $T^+ = 0.7$), medium ($T^+ = 10$ and $T^+ = 25$), and long ($T^+ = 100$ and $T^+ = 200$). This selection of T^+ values ensures that a broad range of turbulence events is targeted.

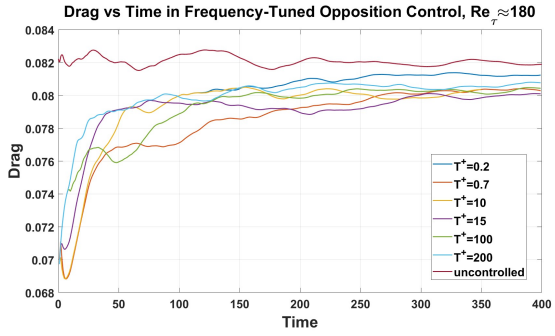

Fig. 9 Temporal evolution of drag, $\mathrm{Re}_\tau \approx 180$

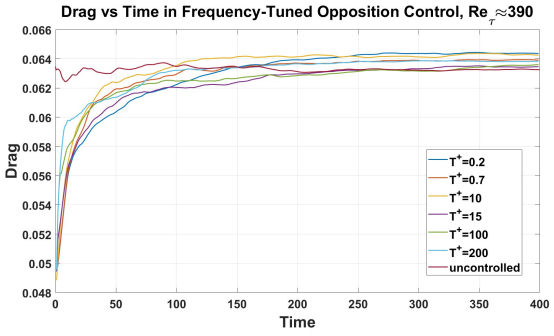

Fig. 10 Temporal evolution of drag, $\mathrm{Re}_\tau \approx 390$

The final drag reduction values for the frequency-tuned opposition control method are presented in Table 1 and Table 2. At $\mathrm{Re}_\tau \approx 180$, the drag reductions are generally minimal, irrespective of the T^+ value of the associated turbulent events, ranging from 1% to 2%. Conversely, at $\mathrm{Re}_\tau \approx 390$, a slight increase in drag is observed, typically between 1% and 2%. This increase can be attributed to the limitations of the single-frequency approach, which proves insufficient to effectively mitigate the more chaotic turbulence events characteristic of higher Reynolds numbers.

Case	T^+	Drag Reduction (%)
1	0.2	0.98%
2	0.7	2.07%
3	10	1.59%
4	25	1.59%
5	100	1.95%
6	200	1.46%

Table 1 Cases with corresponding T^+ values and % drag reduction for $\mathrm{Re}_\tau \approx 180$

Case	T^+	Drag Reduction (%)
1	0.2	-1.73%
2	0.7	-0.95%
3	10	-1.42%
4	25	-0.32%
5	100	-0.47%
6	200	-0.79%

Table 2 Cases with corresponding T^+ values and % drag reduction for $\mathrm{Re}_\tau \approx 390$

D. Frequency-tuned wall-sensing control

Similar to the opposition control method, the results from the wall-sensing method, showing the evolution of drag over time for $Re_\tau \approx 180$ and $Re_\tau \approx 390$, are shown in Figures (11) and (12). Using the same normalization $K = \alpha \cdot A$, $\alpha = 10^{-3}$, as in the untuned wall-sensing control, allowed us to execute the filtered-frequency control with $A = 1000$ (for all cases), resulting in the net control gain $K = 1$. We analyze the frequencies corresponding to six T^+ values for both Reynolds number regimes, the same as in Section IV.C, as presented in Table 3 and Table 4. This selection of T^+ values ensures that a broad range of turbulence events is considered, as done for the opposition control.

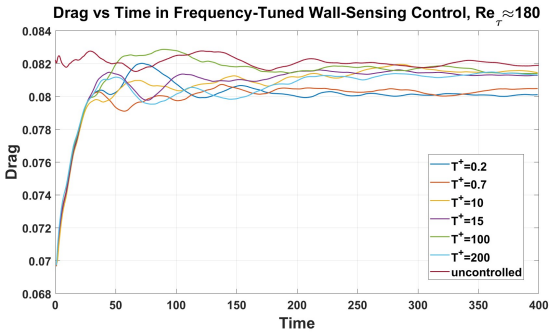

Fig. 11 Temporal evolution of drag, $\mathrm{Re}_\tau \approx 180$

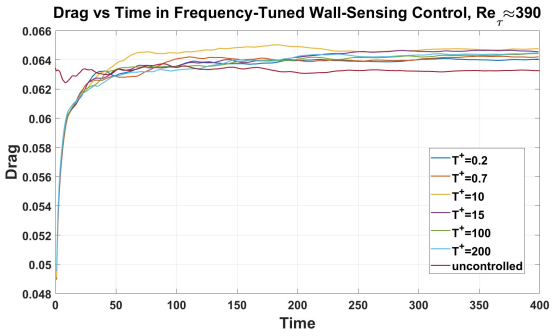

Fig. 12 Temporal evolution of drag, $\mathrm{Re}_\tau \approx 390$

The final drag reduction values for the frequency-tuned wall-sensing method are presented in Table 3 and Table 4. At $\mathrm{Re}_\tau \approx 180$, for all T^+ values and their associated turbulent events, the drag reductions remain minimal, similar to those observed with the frequency-tuned opposition control method, ranging from 1% to 2%. Conversely, at $\mathrm{Re}_\tau \approx 390$, the results indicate a drag increase of 1% to 2%, consistent with what we observed in the frequency-tuned opposition control method.

Case	T^+	Drag Reduction (%)
1	0.2	2.31%
2	0.7	1.83%
3	10	0.73%
4	25	0.85%
5	100	0.73%
6	200	0.85%

Table 3 Cases with corresponding T^+ values and % drag reduction for $\mathrm{Re}_\tau \approx 180$

Case	T^+	Drag Reduction (%)
1	0.2	-1.10%
2	0.7	-1.42%
3	10	-2.35%
4	25	-1.89%
5	100	-1.73%
6	200	-1.89%

Table 4 Cases with corresponding T^+ values and % drag reduction for $\mathrm{Re}_\tau \approx 390$

These results from both the frequency-tuned methods show that the use of a single extracted frequency results is inefficient and results in low drag reductions and for higher turbulence, even drag increment. Hence, we need a banded-frequency approach, where, instead of a single frequency, a band of allowable frequencies will be chosen. This can be implemented either by introducing a band-pass filter function into the inverse Fourier transform in Eq. (4) instead of a delta-function, or by convolving the temporal signal with a corresponding band-pass filter in the time domain.

V. Conclusion

This study investigated a frequency-tuned approach to wall transpiration control to improve the stability and efficacy of turbulent flow management. By selectively targeting specific frequency bands in the wall shear stress signal, the method sought to overcome limitations of existing strategies, particularly the instability caused by high-frequency components in wall-sensing techniques.

A comparative evaluation revealed distinct trade-offs between control strategies. Classical opposition control achieved substantial drag reductions of 21.11% and 18% at $\mathrm{Re}_\tau \approx 180$ and $\mathrm{Re}_\tau \approx 390$, respectively, by leveraging the entire velocity fluctuation spectrum. In contrast, the untuned wall-sensing method achieved smaller reductions of 10.64% and 7.12% but required stabilization measures like freezing the control input. The frequency-tuned approach, however, delivered minimal drag reductions of 1% to 2% and, at $\mathrm{Re}_\tau \approx 390$, even caused a drag increase of 1% to 2%, underscoring the inadequacy of single-frequency control for handling the increased turbulence at higher Reynolds numbers.

These findings emphasize the need for further development of frequency-tuned methods. Future efforts will focus on creating banded-frequency approaches that target a broader range of turbulence dynamics, potentially using band-pass filters or convolution-based time-domain techniques. Such advancements are expected to enhance the stability and performance of both wall-sensing and opposition frequency-tuned control methods.

Acknowledgements

This work was supported by the US Air Force Office of Scientific Research, with Dr. Gregg Abate as the program manager. Partial support of this work by NSF CBET-1944568 grant is also acknowledged.

References

[1] Choi, H., Moin, P., and Kim, J., "Active turbulence control for drag reduction in wall-bounded flows," *Journal of Fluid Mechanics*, Vol. 262, 1994, p. 75–110. https://doi.org/10.1017/S0022112094000431.

[2] M. Schatz, R. P., F. Thiele, and Nitsche, W., "Separation control by periodic excitation and its application," *2nd AIAA Flow Control Conference*, 2004, p. 2507. https://doi.org/10.2514/6.2004-2507.

[3] Huang, L., Huang, P., LeBeau, R., and Hauser, T., "Numerical study of blowing and suction control mechanism on NACA0012 airfoil," *Journal of Aircraft*, Vol. 41, No. 5, 2004, pp. 1005–1013.

[4] Kang, S., and Choi, H., "Active wall motions for skin-friction drag reduction," *Physics of Fluids - PHYS FLUIDS*, Vol. 12, 2000, pp. 3301–3304. https://doi.org/10.1063/1.1320833.

[5] Zhang, S., and Zhong, S., "Turbulent flow separation control over a two-dimensional ramp using synthetic jets," *AIAA journal*, Vol. 49, No. 12, 2011, pp. 2637–2649.

[6] You, D., and Moin, P., "Active control of flow separation over an airfoil using synthetic jets," *Journal of Fluids and Structures*, Vol. 24, No. 8, 2008, pp. 1349–1357.

[7] Cerretelli, C., and Kirtley, K., "Boundary layer separation control with fluidic oscillators," *Journal of Turbomachinery*, Vol. 131, No. 4, 2009, p. 041001.

[8] el Hak, M. G., "Compliant coatings for drag reduction," *Progress in Aerospace Sciences*, Vol. 38, No. 1, 2002, pp. 77–99. https://doi.org/https://doi.org/10.1016/S0376-0421(01)00020-3, URL https://www.sciencedirect.com/science/article/pii/S0376042101000203.

[9] Hussein, M. I., Biringen, S., Bilal, O. R., and Kucala, A., "Flow stabilization by subsurface phonons," *Proceedings of the Royal Society A: Mathematical, Physical and Engineering Sciences*, 2015. https://doi.org/10.1098/rspa.2014.0928.

[10] Kianfar, A., and Hussein, M. I., "Phononic-subsurface flow stabilization by subwavelength locally resonant metamaterials," *New Journal of Physics*, Vol. 25, No. 5, 2023, p. 053021.

[11] Subedi, A., and Peet, Y., "Turbulent Flow Control using Wall-Sensing," AIAA Paper 4030817, 2024. In AIAA Aviation Conference, Las Vegas, NV.

[12] Deville, M. O., Fischer, P. F., and Mund, E. H., "High-Order Methods for Incompressible Fluid Flow," *Applied Mechanics Reviews*, Vol. 56, No. 3, 2003, pp. B43–B43. https://doi.org/10.1115/1.1566402, URL https://doi.org/10.1115/1.1566402.

[13] Fischer, P. F., "An Overlapping Schwarz Method for Spectral Element Solution of the Incompressible Navier Stokes Equations," *Journal of Computational Physics*, Vol. 133, No. 1, 1997, pp. 84–101. https://doi.org/10.1006/jcph.1997.5651.

[14] Fischer, P., Lottes, J., Kerkemeier, S., Marin, O., Heisey, K., Obabko, A., Merzari, E., and Peet, Y., "Nek5000: User's manual," *ANL Report No. ANL/MCS-TM-351*, 2015. Availabel on https://nek5000.mcs.anl.gov/.

[15] Moser, R., Kim, J., and Mansour, N., "Direct numerical simulation of turbulent channel flow up to Re_τ=590," *Physics of Fluids*, Vol. 11, 1999, pp. 943–945. https://doi.org/10.1063/1.869966.

[16] Hammond, E. P., Bewley, T. R., and Moin, P., "Observed mechanisms for turbulence attenuation and enhancement in opposition-controlled wall-bounded flows," *Physics of Fluids*, Vol. 10, No. 9, 1998, pp. 2421–2423.

[17] Chang, Y., Collis, S. S., and Ramakrishnan, S., "Viscous effects in control of near-wall turbulence," *Physics of Fluids*, Vol. 14, No. 11, 2002, pp. 4069–4080.

[18] Chung, Y. M., and Talha, T., "Effectiveness of active flow control for turbulent skin friction drag reduction," *Physics of Fluids*, Vol. 23, No. 2, 2011.